

Wakes of ram pressure stripped disc galaxies

Elke Roediger* and Marcus Brüggen* and Matthias Hoeft*

International University Bremen, P.O. Box 750 561, 28725 Bremen, Germany

Accepted. Received; in original form

ABSTRACT

Spiral galaxies that move through the intracluster medium lose a substantial amount of their gas discs due to ram pressure stripping. The recent observations of NGC 4388 by Oosterloo & van Gorkom (2005) reveal a tail of stripped gas of ~ 100 kpc behind the source galaxy. We present first 3D hydrodynamical simulations of the evolution of such ram pressure stripped tails.

We find that if the ICM wind does not vary significantly over a period of a few 100 Myr, subsonic galaxies produce a tail with regular features similar to a von-Karman vortex street. In this case, the tail widens systematically by about 45 kpc per 100 kpc distance behind the source galaxy. The widening rate is independent of the galaxy's inclination for a large range of inclinations. For supersonic galaxies, the tail is more irregular than for subsonic ones.

The tail observed for NGC 4388 is narrower than the tails in our simulations. Reasons for this difference may be additional physical processes such as heat conduction or viscosity. In addition, we conclude that the observed S-shape of this tail is not due to von Karman oscillations, because this galaxy is likely to move supersonically. A reason for the observed shape may be motions in the ambient ICM.

Finally, we discuss implications for the distribution of metals in the ICM due to ram pressure stripping.

Key words: galaxies: spiral – galaxies: evolution – galaxies: ISM – intergalactic medium

1 INTRODUCTION

Ram pressure stripping, i.e. the removal of a galaxy's gas disc due to its motion through the intracluster medium (ICM), has been studied mainly with regard to the effect on the galaxy (e.g. Abadi et al. 1999; Quilis et al. 2000; Schulz & Struck 2001; Vollmer et al. 2001; Marcolini et al. 2003; Roediger & Hensler 2005; Roediger & Brüggen 2006). It has been shown that the interaction between the ICM and the galactic interstellar medium (ISM) can remove a significant amount of gas from galaxies near cluster centres. Thus, ram pressure stripping is a good candidate to explain observations such as the HI deficiency of cluster disc galaxies (see e.g. Cayatte et al. 1990, 1994; Solanes et al. 2001) and the truncated star forming discs in the Virgo cluster (Koopmann & Kenney 1998, 2004a,b; Koopmann et al. 2005). A distinct feature of ram pressure stripped galaxies is that their gas discs are distorted or truncated while their stellar discs appear undisturbed, because ram pressure stripping affects only the gaseous components of the galaxy. Such examples have been observed, e.g. NGC

4522 (Kenney & Koopmann 1999, 2001; Kenney et al. 2004, Vollmer et al. 2004), NGC 4548 (Vollmer et al. 1999), NGC 4848 (Vollmer et al. 2001). In addition to the effect on the galaxy, ram pressure stripping plays an important role in the evolution of the ICM because the gas lost by galaxies enriches the ICM with metals (see e.g. Schindler et al. 2005; Domainko et al. 2005 and references therein).

A further example of ram pressure stripped galaxies is the Virgo spiral NGC 4388. It has a small distance to the cluster centre and a high radial velocity (~ 1400 km s $^{-1}$) with respect to the cluster mean (see Vollmer & Huchtmeier 2003 and references therein). There is strong evidence that it has suffered ram pressure stripping in its recent history. It was observed to be HI deficient by Cayatte et al. (1990). Moreover, both, ionised and neutral gas have been found at a few kpc distance (also see Vollmer & Huchtmeier 2003 for further references). Vollmer & Huchtmeier (2003) reported the detection of atomic gas at a projected distance of more than 20 kpc from the galactic centre. This extraplanar gas is interpreted as the tail of gas stripped from NGC 4388. On the basis of sticky particle simulations, Vollmer & Huchtmeier (2003) concluded that the main morphological features and velocity structure of NGC 4388 and

* E-mail: e.roediger@iu-bremen.de; m.brueggen@iu-bremen.de; m.hoeft@iu-bremen.de

the extragalactic gas clouds can be explained by ram pressure stripping.

Recently, Oosterloo & van Gorkom (2005) presented observations of a ~ 120 kpc long tail of HI gas associated with NGC 4388, and also suggest that this tail is due to ram pressure stripping of this galaxy, either in the ICM of the Virgo cluster or in the halo of the nearby elliptical galaxy M86. Two prominent features of the tail are its flaring width and its slight S-shape.

Although ram pressure stripping has been studied by several groups, only very few investigations of the resulting gas tails are available. Stevens et al. (1999) and Acreman et al. (2003) simulated ram pressure stripping of hot gas halos from spherical galaxies. They predicted that bow shocks and a tail of hot material will be observable in X-rays. Both groups used cylindrical 2D hydro codes for their simulations.

To our knowledge, so far no simulations of tails of cool gas stripped from disc galaxies have been presented. However, the physics that determines the dynamics of such tails is complex and interesting:

- According to basic hydrodynamics, any object that moves through a fluid produces a wake. The characteristics of this wake depend on the Reynolds number (see any hydrodynamics text book, e.g. Batchelor 2000). For small Reynolds numbers ($Re \lesssim 50$), the wake is thin. For moderate Reynolds numbers ($Re \sim 100$), features similar to the von Karman vortex street develop. The wake’s width can reach several times the width of the body. For high Reynolds numbers ($Re \sim 1000$), the wake becomes turbulent. Especially for moderate and high Reynolds numbers, the wake widens significantly with increasing distance to the object. The value of the Reynolds number in the ICM is a matter of ongoing debate (see e.g. Reynolds et al. 2005), with a large range of values suggested.

- The slight S-shape of the tail of NGC 4388 present in the observation of Oosterloo & van Gorkom (2005) is reminiscent of a von Karman vortex street. However, classical von Karman vortex streets are usually generated behind “2D bodies”, like cylinders, that force the flow into a translational symmetry along the axis of the body. In contrast, the flow past a galaxy is a full 3D flow and thus possesses a more complex wake structure.

- The stripping process alone may lead to a widening of the galaxy’s tail because the ICM is forced to flow around the galactic gas disc. Therefore, the galactic gas can acquire velocity components perpendicular to the main ICM wind direction.

- Additions to the dynamics in the galactic wake/tail could arise from the rotation of the disc gas. As the stripped galactic gas moves away from the galaxy, the radial gravitational acceleration ceases to operate on the stripped gas. In the extreme case of a face-on galaxy where the radial acceleration is simply switched off, a stripped gas package would move linearly with $v = v_{\text{rot}}$ perpendicular to \vec{v}_{ICM} from that moment on. The ICM wind can accelerate the stripped gas package to maximal v_{ICM} in wind direction. The superposition of a motion with v_{ICM} in wind direction and v_{rot} in any direction perpendicular to this would lead to a widening angle of $\alpha = 2 \arctan(v_{\text{rot}}/v_{\text{ICM}})$. This process should be inclination-dependent. Of course, stripped gas has to pass a

transition region where the radial gravitational acceleration ceases to operate.

- The inclination angle between the galactic rotation axis and the galaxy’s direction of motion may influence the wake due to geometrical reasons alone, i.e. the effective cross-section of the “obstacle” in the ICM wind changes. Furthermore, the flow patterns of subsonic and supersonic cases are expected to differ because in supersonic cases a bow shock develops.

Most of the aspects listed above require a 3D treatment of the problem. Here, we present first 3D hydrodynamical adaptive-mesh simulations of the evolution of tails of ram pressure stripped galaxies.

2 METHOD

We study the motion of the galaxy through the cluster in the rest frame of the galaxy. Therefore, its motion translates into an ICM wind flowing past the galaxy.

2.1 Code

The simulations were performed with the FLASH code (Fryxell et al. 2000), a multidimensional adaptive mesh refinement code. It solves the Riemann problem on a Cartesian grid using the Piecewise-Parabolic Method (PPM), which is particularly well suited to resolve shocks. The gas obeys a polytropic equation of state with an adiabatic index of $\gamma = 5/3$. All boundaries but the inflow boundary are open. The simulations presented here are performed in 3D. In order to follow the evolution of the wake, we use a large simulation box of size $(x_{\text{min}}, x_{\text{max}}) \times (y_{\text{min}}, y_{\text{max}}) \times (z_{\text{min}}, z_{\text{max}}) = (-162 \text{ kpc}, 162 \text{ kpc}) \times (-64 \text{ kpc}, 260 \text{ kpc}) \times (-162 \text{ kpc}, 162 \text{ kpc})$ for subsonic cases and $(-121.5 \text{ kpc}, 121.5 \text{ kpc}) \times (-64 \text{ kpc}, 260 \text{ kpc}) \times (-121.5 \text{ kpc}, 121.5 \text{ kpc})$ for supersonic ones. The galactic centre is located at $(x_{\text{gal}}, y_{\text{gal}}, z_{\text{gal}}) = (0, 0, 0)$. The ICM wind is flowing along the y -axis into the positive direction. We use 6 levels of refinement, which leads to an effective resolution of 316.5 pc and an effective number of grid cells of $(1024)^3$ for the subsonic cases. However, at a distance of more than 64 kpc behind the galaxy (behind=downstream) we limit the effective resolution to 633 pc (5 levels of refinement) to limit computational costs. For the same reason, the number of refinement levels is restricted to 5 for the supersonic runs, where a multitude of shocks and waves causes massive refinement (see Fig. 2). The refinement criteria are the standard density and pressure gradient criteria. The galactic disc is always refined.

In order to be able to identify the galactic gas after it is stripped from the galaxy, we use a “dyeing” technique: The FLASH code offers the opportunity to advect mass scalars along with the density. We utilise one of these mass scalars, f , to contain the fraction of galactic gas in each cell. Initially this array has the value 1 in the region of the galactic disc and 0 elsewhere. As a result, every cell where $f > 0$ contains a certain amount of gas that has originally been inside the galaxy. At each timestep, the quantity $f\rho$ gives the local density of galactic gas.

Table 1. Galaxy model parameters.

stellar disc	M_*	$10^{11} M_\odot$
	a_*	4 kpc
	b_*	0.25 kpc
bulge	M_{bulge}	$10^{10} M_\odot$
	r_{bulge}	0.4 kpc
DM halo	r_{DM}	23 kpc
gas disc	M_{gas}	$10^{10} M_\odot^*$
	a_Σ	7 kpc
	b_{gas}	0.4 kpc
	v_{rot}	200 km s $^{-1}$

2.2 Model galaxy

We model a massive spiral galaxy with a flat rotation curve at 200 km s $^{-1}$. It consists of a gas disc, a stellar disc, a stellar bulge and a dark matter (DM) halo. For the gravitational potential of the stellar disc, bulge and DM halo, we use the following analytical descriptions:

Stellar disc: Plummer-Kuzmin disc, see Miyamoto & Nagai (1975) or Binney & Tremaine (1987). Such discs are characterised by their mass, M_* , and radial and vertical scale lengths, a_* and b_* , respectively.

Stellar bulge: Spherical Hernquist bulge (see Hernquist 1993). In case of a spherical bulge, the gravitational potential, Φ , depends on radius, r , as $\Phi(r) = -\frac{GM_{\text{bulge}}}{r+r_{\text{bulge}}}$, where M_{bulge} is the mass of the bulge, r_{bulge} the scale radius and r the spherical radius.

DM halo: The spherical model of Burkert (1995), including the self-scaling relations, i.e. the DM halo is characterised by the radial scale length, r_{DM} , alone. For the equation of the analytical potential see also Mori & Burkert (2000).

The self-gravity of the gas is neglected as the gas contributes only a small fraction to the overall galactic mass. The parameters of our galaxy model are summarised in Table 1. In order to prevent steep density gradients in the galactic plane and in the galactic centre, the gas disc is described by a softened exponential disc :

$$\rho(R, Z) = \frac{M_{\text{gas}}}{2\pi a_{\text{gas}}^2 b_{\text{gas}}} 0.5^2 \operatorname{sech}\left(\frac{R}{a_{\text{gas}}}\right) \operatorname{sech}\left(\frac{|Z|}{b_{\text{gas}}}\right). \quad (1)$$

The coordinates (R, Z) are galactic cylindrical coordinates. The radial and vertical scale lengths are a_{gas} and b_{gas} , respectively. For $R \gtrsim a_{\text{gas}}$ and $|Z| \gtrsim b_{\text{gas}}$, this density distribution converges towards the usual exponential disc $\rho(R, Z) = \frac{M_{\text{gas}}}{2\pi a_{\text{gas}}^2 b_{\text{gas}}} \exp(-R/a_{\text{gas}}) \exp(-|Z|/b_{\text{gas}})$. For the corresponding exponential disc, M_{gas} is the total gas mass. We chose M_{gas} such that in the outer regions the gas disc converges to an exponential gas disc with 10% of the stellar disc mass, i.e. $M_{\text{gas}} = 0.1M_*$. The integrated gas mass amounts to $6 \cdot 10^9 M_\odot$. Given the density distribution in the disc, its pressure and temperature distribution are set such that hydrostatic equilibrium with the ICM is maintained in the direction perpendicular to the disc plane. In radial direction, the disc's rotation velocity is set so that the centrifugal force balances the gravitational force and pressure gradients. We have cut the gas disc smoothly to a finite radius of 26 kpc by multiplying the density distribution $\rho(R, Z)$ with

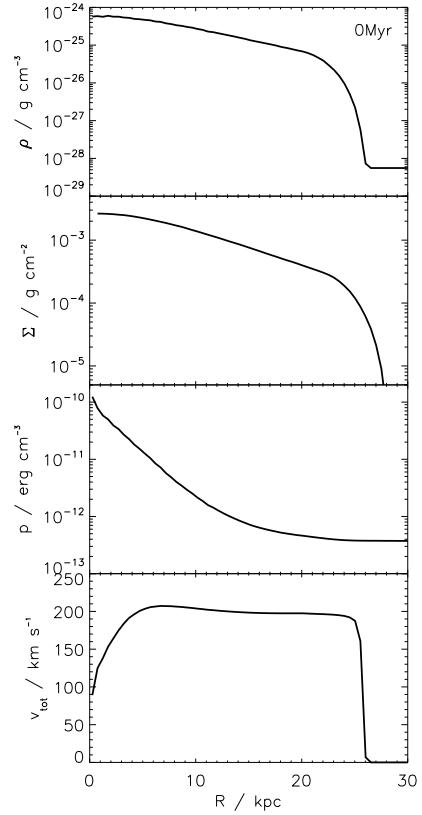

Figure 1. Radial profiles of the density, ρ , pressure, p , and rotation velocity, v_{rot} , in the galactic plane for the initial model. Also the radial profile for the projected ISM surface density, Σ , is shown.

Table 2. ICM wind parameters. Ram pressure p_{ram} , ICM wind density ρ_{ICM} , ICM wind velocity v_{ICM} , inclination angle i .

$p_{\text{ram}}/$ (erg cm $^{-3}$)	$\rho_{\text{ICM}}/$ (g cm $^{-3}$)	$v_{\text{ICM}}/$ (km s $^{-1}$)	$i/^\circ$
$6.4 \cdot 10^{-11}$	10^{-26}	800	30
$6.4 \cdot 10^{-11}$	10^{-27}	2530	30
$6.4 \cdot 10^{-12}$	10^{-27}	800	30, 75
$6.4 \cdot 10^{-12}$	10^{-28}	2530	30

$0.5[1 + \cos(\pi(R - 20 \text{ kpc})/6 \text{ kpc})]$ for $20 \text{ kpc} < R \leq 26 \text{ kpc}$. Figure 1 shows radial profiles of density, surface density, pressure and rotation velocity for the initial model.

We measure the inclination angle, i , of the galaxy as the angle between its rotation axis and the ICM wind direction. Thus 0° corresponds to a face-on motion of the galaxy, and 90° to edge-on.

2.3 ICM conditions

For a first experiment, we expose model galaxies to constant ICM winds. We list p_{ram} , v_{ICM} , ρ_{ICM} and inclination angle, i , in Table 2. We chose the ICM temperature such that the sound speed is 1000 km s $^{-1}$. We refer to the two ram pressures as medium ($p_{\text{ram}} = 6.4 \cdot 10^{-12}$ erg cm $^{-3}$) and strong ($p_{\text{ram}} = 6.4 \cdot 10^{-11}$ erg cm $^{-3}$) ram pressure. For both

ram pressures, we test a subsonic ($v_{\text{ICM}} = 800 \text{ km s}^{-1}$, Mach number 0.8) and a supersonic ($v_{\text{ICM}} = 2530 \text{ km s}^{-1}$, Mach number 2.53) case.

For the subsonic runs, we start with the ICM at rest and then increase the inflow velocity during the first 50 Myr. For the supersonic runs, this procedure takes too long until a true supersonic flow including a bow shock develops. Therefore, for supersonic runs, we set v_{ICM} everywhere in the ICM already initially. In this procedure, the simulation starts a bit violently, but after a bit less than 100 Myr a true bow shock has developed. This difference in initialisation leads to a temporal offset between subsonic and supersonic runs. A time t in a supersonic run corresponds to approximately $t + 50 \text{ Myr}$ in a subsonic run.

3 RESULTS

3.1 Snapshots in slices

Figure 2 shows the gas density distribution in a slice through the simulation box parallel to the y - z -plane at $x = 0$ for different timesteps for the case of medium ram-pressure and supersonic ICM flow. In addition to the bow shock, the stripped material induces a rich shock structure in the region behind the bow shock. The stripped material fragments strongly due to turbulence and Rayleigh-Taylor-instability.

3.2 Projected gas densities

In this section, we show projected galactic gas densities along two lines-of-sight for our simulation runs at different timesteps (Figs. 3 to 7). The galactic gas is identified by the mass scalar described in Sec. 2.1. In all figures in this section, the left column shows projections along the x -axis, while the right column shows projections along the z -axis. These are the two directions perpendicular to the direction of motion (which is along the y -axis). The time is denoted in the upper left panel of each snapshot. Each figure caption denotes the ram pressure, Mach number and inclination angle of the run.

All projections of the medium ram-pressure cases show gas tails with column number densities around 10^{19} cm^{-2} . The tails of the high ram-pressure cases have a column density roughly a factor of 10 higher. Typical tail widths are between 60 and 100 kpc.

In the cases with medium ram-pressure, the galaxy can retain a tail for several 100 Myr and the tail can also evolve during this time. In the cases with strong ram-pressure, the complete gas disc is stripped after a few 100 Myr, so that one cannot speak of a galactic tail any more. Instead, the bulk of stripped gas moves downstream as a stretched gas cloud which is few 100 kpc long. The fact that in the high ram-pressure cases much more gas is lost in a shorter time leads to a distribution of more mass into a smaller volume and thus higher column densities in the tails.

3.3 Velocity structure in the tail

Figures 8 to 12 show the velocities of the stripped gas in the wake. For a random, ISM density weighted subset of grid cells, the velocity components in y -, x - and z -direction

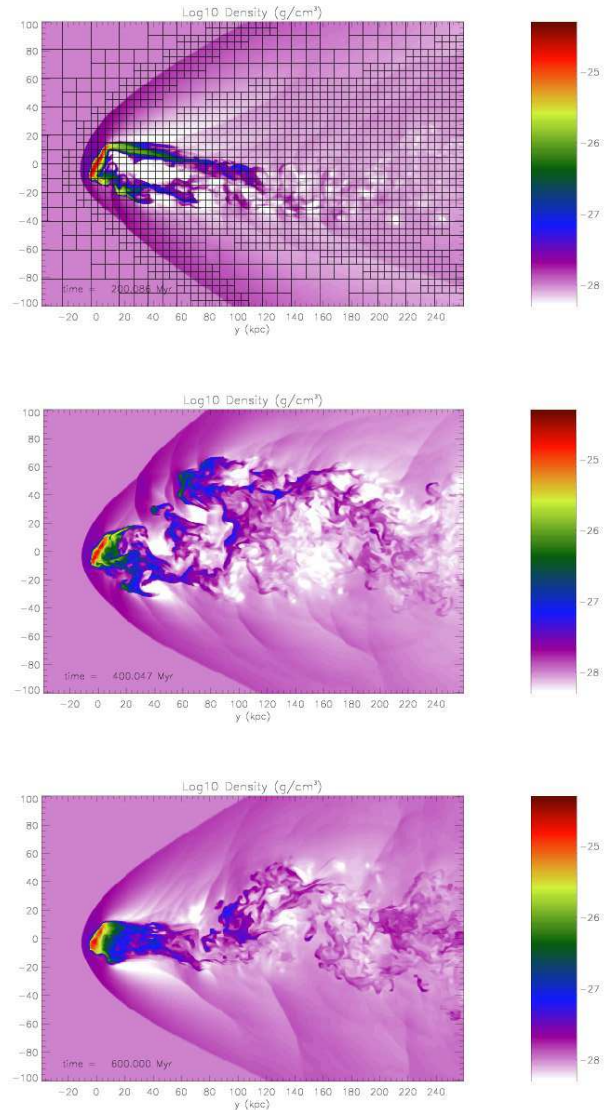


Figure 2. Slice through simulation box in the y - z -plane for the supersonic run with medium ram-pressure and $i = 30^\circ$. The local gas density is shown colour-coded for different time steps. The refinement is demonstrated in the first plot, one square shows the size of one block = 8^3 grid cells.

are plotted as a function of distance to the galaxy. In our simulations, v_y is the velocity component in wind direction, whereas v_x and v_z are perpendicular to the wind direction. The caption of each figure denotes the ram pressure, Mach number and inclination angle of the run.

The component v_y reflects the acceleration of the stripped gas in the wind direction. The components perpendicular to the wind direction cannot result solely from galactic rotation. In the panels for the v_x - and v_z -components, we have marked the amplitude of the galactic rotation velocity $v_{\text{rot}} = \pm 200 \text{ km s}^{-1}$. If the stripped gas were pushed straight into the wind direction, no velocities higher than this should occur in v_x and v_z . But in all cases velocities higher than the galactic rotation occur. Especially in the 75° case, the galactic rotation induces only a small v_z -component. Almost all

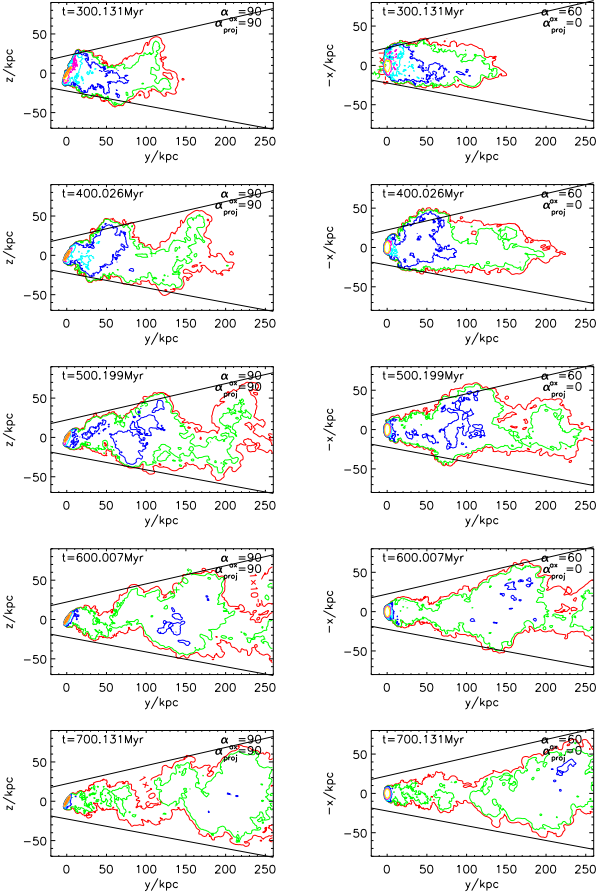


Figure 3. Projected galactic gas density for medium ram-pressure, Mach number 0.8, $i = 30^\circ$. Lowest contour is $10^{-5} \text{g cm}^{-2} \approx 6.0 \cdot 10^{18} \text{cm}^{-2}$. The contour spacing is half an order of magnitude. The left column is for projection along the x -axis, the right column for projection along the z -axis. The time of each panel is denoted in its upper left corner. The two numbers in the upper right corner denote the projection direction with respect to the galaxy: α_{ax} is the angle between the line-of-sight and the galactic rotation axis. If the line-of-sight is projected into the grid's x - z -plane, the resulting line has an angle of α_{proj} with the negative part of the grid's z -axis. α_{ax} and α_{proj} are given in degree.

of the observed v_z must be due to the ICM flow. The excess in v_x and v_z arises because the ICM is flowing smoothly around the galaxy. Thus, already the ICM flow near the galaxy contains velocity components in x - and z -direction. In the supersonic case, the oblique bow shock also leads to non-zero v_x - and v_z -components. The strongest increase of v_x and v_z is observed in the supersonic case. Additional excess in v_x and v_z is introduced by turbulence.

The velocity width in the tail also differs in subsonic and supersonic cases. The overall width in the subsonic cases is $\sim 400\text{-}600 \text{km s}^{-1}$, whereas in the supersonic cases it is nearly twice as much. The velocity width is roughly independent of ram pressure.

Interestingly, in the subsonic cases, oscillations appear in v_x and especially in v_z . Their origin is discussed below.

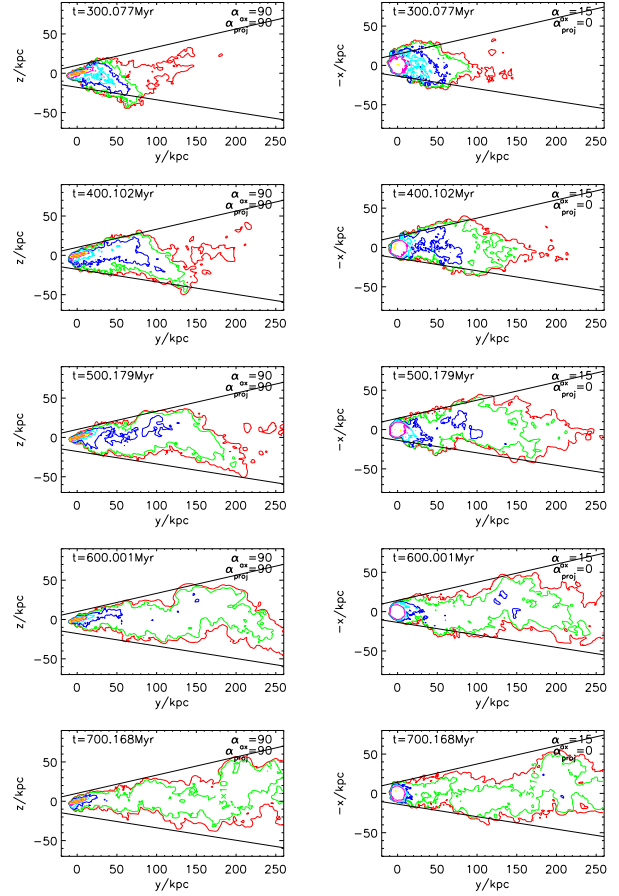


Figure 4. Projected galactic gas density for medium ram-pressure, Mach number 0.8, $i = 75^\circ$. Otherwise same as Fig. 3.

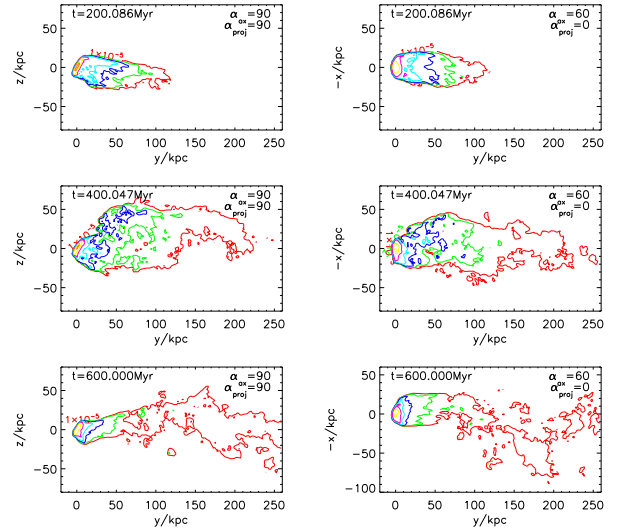


Figure 5. Projected galactic gas density for medium ram-pressure, Mach number 2.53, $i = 30^\circ$. Otherwise same as Fig. 3.

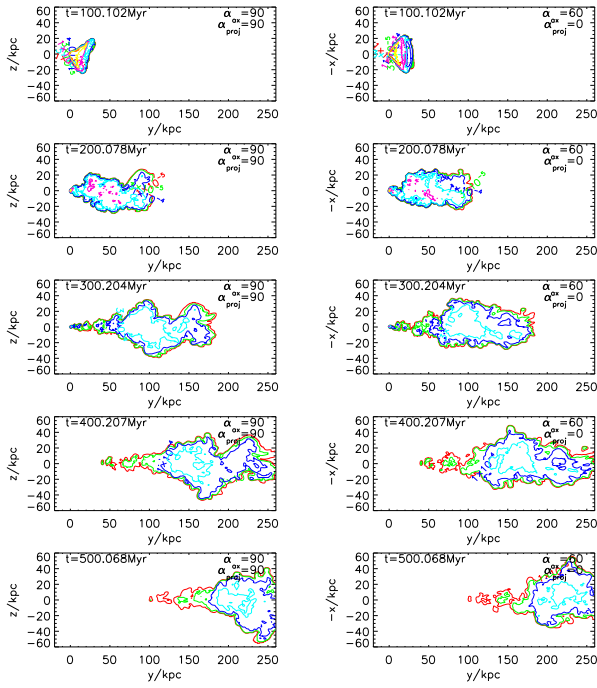


Figure 6. Projected galactic gas density for strong ram-pressure, Mach number 0.8, $i = 30^\circ$. Otherwise same as Fig. 3. In the lower panels, the bulk of stripped gas can be seen to move away from the galaxy (the galactic centre is located at $(x, y, z) = (0, 0, 0)$ for all timesteps).

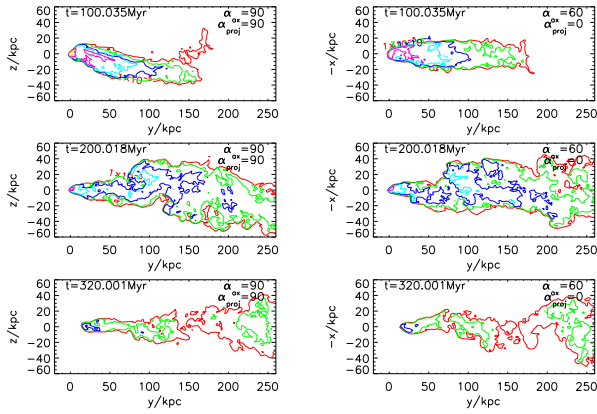


Figure 7. Projected galactic gas density for strong ram-pressure, Mach number 2.53, $i = 30^\circ$. Otherwise same as Fig. 3.

3.4 Tail structure

The shape of the tail depends mainly on Mach number. Only in the subsonic cases regular structures similar to a von Karman vortex street can be produced (see Figs. 3 and 4). The formation of a long regular tail also takes several 100 Myr. Therefore, less regular structure is produced in the strong ram-pressure run because the gas disc is already stripped completely after a few 100 Myr. Moreover, in Fig. 3, an oscillating tail appears in the projection along the x -axis, but not along the z -axis. If we neglect the disc rotation for the moment, then the galaxy appears asymmetrical due to its inclination only in z -direction, but not in x -direction. Therefore, the “von Karman oscillations” are more prominent in

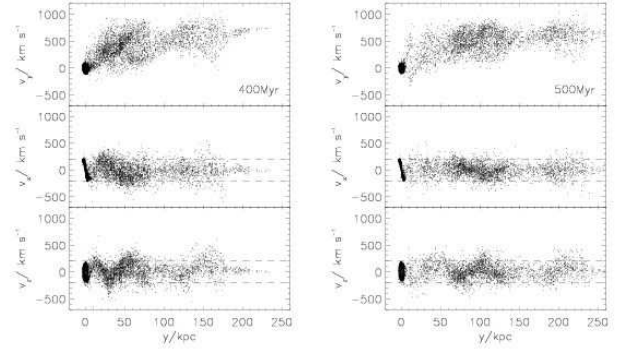


Figure 8. Velocity components in the wake, for medium ram-pressure, Mach number 0.8, $i = 30^\circ$. The top panels shows the velocity along wind direction (y -axis), the middle and bottom panels show the velocity components in the two directions perpendicular to the wind direction (x - and z -direction). Each column is for one timestep. The time is denoted in the top panel of each column. The dashed vertical lines in the middle and bottom panels denote the amplitude of galactic rotation.

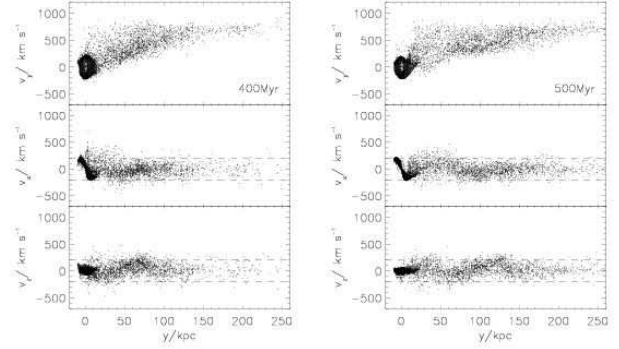


Figure 9. Velocity components in the wake, for medium ram-pressure, Mach number 0.8, $i = 75^\circ$. Otherwise same as Fig. 8.

z -direction, and hence can be seen best if the line-of-sight is the x -axis. Also the oscillations observed in the velocity components perpendicular to the wind direction v_x and v_z (see Sect. 3.3) are connected to the “von Karman oscillations”.

The supersonic cases show an irregular tail structure.

3.5 Flaring of the wake

In addition to the von-Karman oscillations, in the subsonic cases the tail widens systematically although this effect is less prominent in the high ram-pressure case because the gas disc is already stripped completely at early times. The velocity components perpendicular to the wind direction are similar for, both, the medium and high ram-pressure case. Therefore, the tail is slightly narrower in the stronger ram-pressure case because here the stripped gas is accelerated faster.

In the subsonic, medium ram-pressure cases, the widening proceeds roughly linearly on the length scale of our simulation box. The tail width ranges from a few 10 kpc near the galaxy to 150 kpc at the end of the simulation box (distance of 260 kpc behind the galaxy). The diagonal lines in

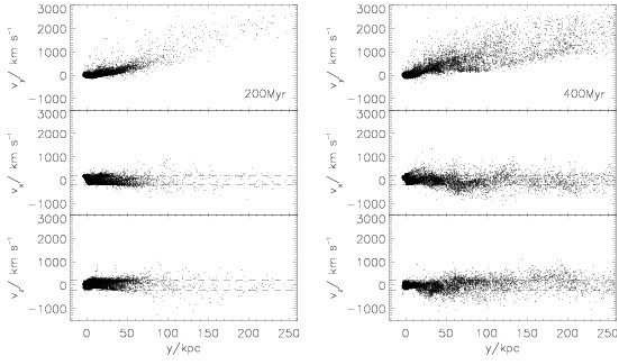


Figure 10. Velocity components in the wake, for medium ram pressure, Mach number 2.53, $i = 30^\circ$. Otherwise same as Fig. 8.

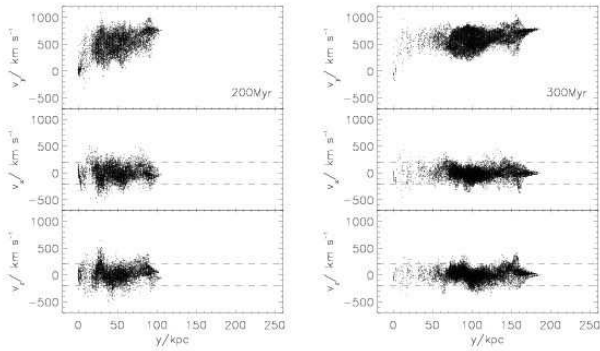


Figure 11. Velocity components in the wake, for strong ram pressure, Mach number 0.8, $i = 30^\circ$. Otherwise same as Fig. 8.

Figs. 3 and 4 envelop the tail. They were fitted by eye. In each figure, they are identical for all panels, i.e. they are independent of time and projection direction.

The difference in the angles of the envelopes between the two inclinations is very small. However, for the more highly inclined galaxy, the enveloping lines are closer together. For higher inclinations, the width of the tail at a given distance to the galaxy is smaller. In both inclinations, the upper envelope has an angle of 13° with respect to the y -axis. The angles between the lower envelope and the y -axis are 9° and 10.5° for the inclinations of 75° and 30° , respec-

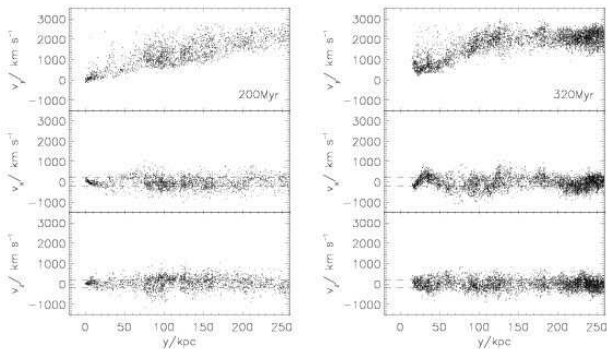


Figure 12. Velocity components in the wake, for strong ram pressure, Mach number 2.53, $i = 30^\circ$. Otherwise same as Fig. 8.

tively. For the projections along the z -axis (right column) the different angles between the lower and upper line could be explained by the disc’s rotation. In these panels, the disc is rotating counter-clockwise. Therefore, at the bottom side of the panel, the disc is rotating in wind direction, whereas on the upper side of the panel the disc is rotating antiparallel to the wind direction. This leads to a slightly stronger stripping at the bottom side and a slightly stronger stretching of the bottom side of the tail. For the projection along the x -axis, the reason must be a different one because here the rotation does not induce a similar asymmetry. Here, the inclination makes the galaxy asymmetrical for the ICM flow. Moreover, the stripping process itself proceeds asymmetrically for inclined galaxies (see Roediger & Brüggén 2006). However, it is surprising that the asymmetry of the tail is similar for both inclinations and both projection directions.

The fact that the widening of the tail proceeds in a very similar fashion independent of galactic inclination suggests that the dynamics of the widening are independent of the galaxy but intrinsic to the ICM flow. This also excludes the widening due to the rotation of the disc gas as presumed in the introduction as a major process.

In the supersonic, medium ram-pressure case the tail widens, too, despite its irregular behaviour. The least widening is observed in the supersonic high ram-pressure case. However, the velocity components perpendicular to the wind direction are high in the supersonic case, so that some widening could be observed if the tail is traced to even larger distances behind the galaxy.

4 DISCUSSION

4.1 Observable galactic tails

4.1.1 General

Given that the stripped gas remains in the HI temperature range, our simulations suggest that deep HI observations could observe long galactic tails. For galaxies that experience a strong ram pressure and lose nearly their complete gas disc in a few 100 Myr, the tails could be detected with less sensitive observations. In such cases, the tail can even separate from the source galaxy (see bottom panels of Fig. 6) and appear as a large isolated gas cloud. In addition to the spatial separation, the “tail” gas cloud will also be separated from its source galaxy in velocity space. This makes it very difficult to recognise the original connection between the gas cloud and the source galaxy. An HI survey of the Virgo cluster (Davies et al. 2004) has indeed found two candidates of HI clouds without optical counterparts.

Our simulations predict tail widths in the range of 60 to 100 kpc at *non-projected* distances of ~ 100 kpc behind the galaxy. If a galaxy moves subsonically, if it is exposed to a medium ram pressure and seen along a favourable line-of-sight, even regular structures similar to von-Karman oscillations could be detected. However, some additional processes could modify the appearance of the tails:

- For galaxies passing through cluster centres, the ICM wind will be variable. The decrease of ram pressure after the peak ram pressure and back-falling material could change, both, the tail structure and the structure of the velocity

component in wind direction. The velocity components perpendicular to the wind direction should not be sensitive to this process. However, in observations the components into and perpendicular to wind direction may be difficult to disentangle.

- We neglected cooling and thermal conduction. These processes are important for the question whether the stripped gas stays observable as HI. If a tail is observed during heating or cooling, the structure observed in HI may be completely decoupled from the overall structure of all stripped gas because some parts drop out of the relevant temperature range. However, the observation of Oosterloo & van Gorkom (2005) suggests that at least a part of the stripped gas can survive as HI for a few 100 Myr. More detailed studies are needed to investigate the role of thermal conduction.

- We also neglected viscosity in our simulations. Due to numerical viscosity, our simulations match the case of moderate to high Reynolds numbers. Magnetic fields in the ICM may suppress viscosity significantly, which could lead to higher turbulent velocities and greater widening of the tail. On the other hand, a substantial amount of viscosity would smooth the turbulent structures that develop in our simulations, and galactic tails may be narrower than we predict.

- Local ICM motions as found in many cluster simulations (e.g. Faltenbacher et al. 2005; Takizawa 2005) could deform and bend the galactic tails.

4.1.2 *The case of NGC 4388*

So far, the only example of a long tail of cool ram pressure stripped gas is the case of NGC 4388 in the Virgo Cluster (Oosterloo & van Gorkom 2005). This galaxy's tail has a length of ~ 120 kpc in the plane of the sky, the tail width flares from about 15 kpc near the galaxy to about 40 kpc at a projected distance of 100 kpc behind the galaxy. The ridge of maximum flux density suggests a slight S-shape of the tail.

In order to disentangle the true properties of the wake, the velocity component in the plane of the sky would have to be known. The length of the tail indicates that this component is substantial. The radial velocity of NGC 4388 with respect to the cluster mean is ~ 1400 km s $^{-1}$ (see Vollmer & Huchtmeier 2003 and references therein). Even if this galaxy had no velocity component in the plane of the sky, its radial velocity suggests already a slight supersonic motion through the ICM, which would be enough to qualify this galaxy's velocity as typical for cluster galaxies. Consequently, a substantial velocity component in the plane of the sky as indicated by the long tail suggests that NGC 4388's true velocity with respect to the cluster mean is rather high. Thus, it is very likely that this galaxy is moving supersonically through the ICM. Therefore, our simulations suggest that the implied S-shape in the tail is not due to regular von-Karman oscillations. The observed S-shape could also be coincidental and not part of a regular pattern. In our supersonic simulations situations like this occur, the supersonic tails are far from being perfectly straight. NGC 4388's tail shape may also be caused by other processes discussed above.

Even if the velocity component in the plane of the sky is comparable to the radial component (in the cluster rest

frame), this implies that the true length of the tail is at least 1.4 times as long as the projected one. If the velocity component in the plane of the sky is only ~ 500 km s $^{-1}$, the true tail is about 3 times as long as the projected one. A reasonable assumption for the ICM density at NGC 4388's position is a few 10^{-4} cm $^{-3}$. With an assumed velocity of ~ 1800 km s $^{-1}$ it is likely that this galaxy experienced a ram pressure in the range we studied here. In our simulations, we can reproduce such very long tails. The details of the tail length may also depend on the exact stripping history, i.e. the time dependence of the ram pressure during the cluster passage. Thus, comparisons with simulations of realistic cluster passages that also trace the evolution of the galactic tail may be used to infer the galaxy's proper velocity.

The width of the tail does not depend on the projection direction. Thus, the tail of NGC 4388 is narrower than the tails in our simulations. This difference may be caused by reasons discussed above. E.g. if the ICM is more viscous than in our simulations, the tail will be narrower. Alternatively, some parts of the tail may already have dropped out of the relevant temperature range in order to be observable in HI. Comparisons with simulations including these effects could give important insights on the degree of viscosity and thermal conduction in the ICM.

Oosterloo & van Gorkom (2005) have also measured the radial velocity in the tail of NGC 4388. Close to the galaxy, the radial velocity agrees with the galaxy's radial velocity. Then it decreases along the tail by about 550 km s $^{-1}$. This means that the stripped gas at the end of the tail has reached only about 40% of the galactic radial velocity with respect to the cluster mean. However, it takes some time until the stripped gas is decelerated sufficiently to fall behind the galaxy. In this point, our simulations agree with the observations. Also in our supersonic simulations, the stripped gas does not reach the full ICM wind speed inside our simulation box, and gas at true distances of 100 kpc behind the galaxy has reached only about 50% of v_{ICM} . Again, details of the velocity structure depend on the exact stripping history.

In addition to the velocity decrease, Oosterloo & van Gorkom (2005) have measured the velocity width in the tail. They derive values of 100 to 200 km s $^{-1}$. This is surprisingly low as one would expect the stripped gas to preserve the rotation it had inside the galaxy, i.e. the width should be at least twice the rotation velocity. Our simulations show at least this width, and the supersonic simulations even show a higher width. This is in accord with the simulations of Vollmer & Huchtmeier (2003) that produce velocity widths of ~ 400 km s $^{-1}$. The reason for this discrepancy might be that Oosterloo & van Gorkom (2005) have measured the velocity only along the ridge of highest flux density. Thereby, they may have incidentally selected a special fraction of the tail, like gas that originated from a certain part of the galaxy only.

4.1.3 *Other examples*

To our knowledge, no other long galactic tails have been observed in HI. Some observations exist in other wavelengths. E.g. for CGCG 97-073 and 97-079 in the cluster A1367 $H\alpha$ and radio continuum tails have been detected (see Gavazzi et al. 1995, 2001). Both galaxies show tails of ~ 75 kpc length. The $H\alpha$ tails are rather thin and straight

and show little substructure. The radio continuum tails show a some widening. It will be interesting to observe these galaxies and others in deep HI for further analysis.

4.2 Metal distribution in the ICM due to ram pressure stripping

Gas stripped from galaxies is an important source of metals for the ICM (Schindler et al. 2005; Domainko et al. 2005). Therefore, the evolution of galactic tails plays an important role in the distribution of metals in the ICM. In our simulations, we find that the width of the tails behaves like $w/d \leq 0.4$ (see e.g. Fig. 3), where w is the tail width and d the distance from the galaxy. However, our simulations trace only the first 260 kpc behind the galaxy and the width of the wake is not going to increase linearly with the distance from the galaxy. In a simple model, we can model the turbulent widening of the wake as a diffusion process with a diffusion constant given by $D \approx \frac{1}{3}\sigma l$, where σ is a typical turbulence velocity and l a typical size of turbulence eddies. Our simulations suggest velocity dispersions of $\sigma \sim 250 \text{ km s}^{-1}$ for galactic velocities of $\sim 800 \text{ km s}^{-1}$ to $\sigma \sim 500 \text{ km s}^{-1}$ for galactic velocities of $\sim 2500 \text{ km s}^{-1}$. The typical eddy size, l , in our simulations is $\sim 50 \text{ kpc}$. Thus, the time to reach a certain width w is given by

$$\begin{aligned} t &\sim \frac{1}{4} \frac{w^2}{D} = \frac{3}{4} \frac{w^2}{\sigma l} \\ &= 600 \text{ Myr} \left(\frac{w}{100 \text{ kpc}} \right)^2 \left(\frac{\sigma}{250 \text{ km s}^{-1}} \right)^{-1} \left(\frac{l}{50 \text{ kpc}} \right)^{-1} \end{aligned} \quad (2)$$

During this time, the tail length increases by $\sim v_{\text{ICM}}t$. Consequently, the tail length d and its width relate as

$$\begin{aligned} w &\sim \sqrt{\frac{4dD}{v_{\text{ICM}}}} = \sqrt{\frac{4d\sigma l}{3v_{\text{ICM}}}} \\ &= 130 \text{ kpc} \left(\frac{d}{1 \text{ Mpc}} \right)^{1/2} \left(\frac{v_{\text{ICM}}}{1000 \text{ km s}^{-1}} \right)^{-1/2} \\ &\quad \left(\frac{\sigma}{250 \text{ km s}^{-1}} \right)^{1/2} \left(\frac{l}{50 \text{ kpc}} \right)^{1/2} \end{aligned} \quad (3)$$

This estimate neglects that the turbulence decays as the gas streams away from the galaxy. The decay of turbulence makes, both, σ and l smaller with increasing distance to the galaxy and therefore, the above estimate gives an upper limit on w .

These estimates could be included in future simulations of metal enrichment of the ICM by ram pressure stripping. Some of these simulations inject metals provided certain analytical criteria for ram-pressure stripping are fulfilled. These simulations could be refined by imparting the stripped material with a velocity dispersion to produce more realistic tails.

4.3 Heating of the ICM by turbulence in the wakes

The ongoing search for a heat source in galaxy clusters that prevents catastrophic cooling in the cool cores makes it interesting to estimate the extent to which the motion of galaxies can heat the ICM.

The kinetic energy of a galaxy can heat its ambient

medium via three mechanisms: (i) the flow around the galaxy can lead to turbulence in the wake of the galaxy as seen in our simulations, (ii) dynamical friction accelerates the surrounding gas (Ostriker 199; Kim et al. 2005), and (iii) in case of supersonic motion, the ambient gas is heated by a bow shock. For the first two mechanisms the induced motions need to be converted to heat by some dissipative process.

As the galaxy moves through the ICM, it produces a turbulent wake. The energy loss of the galaxy may be estimated by

$$\left. \frac{dE_{\text{gal}}}{dt} \right|_{\text{ram}} = -p_{\text{ram}} A_{\text{proj}} v_{\text{ICM}}, \quad (4)$$

where A is the projected surface area of the galaxy. Using conservative values, i.e. $p_{\text{ram}} = 6.4 \times 10^{-11} \text{ erg cm}^{-3}$, $v_{\text{ICM}} = 1000 \text{ km s}^{-1}$ and $A = 4\pi(4 \text{ kpc})^2$, we obtain a loss rate $\sim 10^{42} \text{ erg s}^{-1}$. This energy can be found as turbulent energy in the ICM. For about 100 galaxies within a cluster, this heating rate is comparable to the cooling rate by radiative losses.

Also, this heating rate is consistent with what we find in our simulations. A rough inspection of the velocity distribution, see Fig. 2 and 12, shows that the ICM is stirred within a tube of diameter $\sim 40 \text{ kpc}$ with a velocity dispersion of $\sigma_x \sim 400 \text{ km s}^{-1}$. The ICM has an average gas density of $10^{-28} \text{ g cm}^{-3}$ and the galaxy moves with 1000 km s^{-1} through the ICM. This yields a rate of kinetic energy injection of $\sim 10^{42} \text{ erg s}^{-1}$, which is very similar to our estimate above.

It is interesting to compare this result to the energy input by dynamical friction. However, it should be noted that our simulations do not include the effect of dynamical friction (DF) since self-gravity is not included.

$$\left. \frac{dE_{\text{gal}}}{dt} \right|_{\text{DF}} = M_{\text{gal}} v \left. \frac{dv}{dt} \right|_{\text{DF}} = -\frac{4\pi \ln \Lambda G^2 \rho_{\text{ICM}} M_{\text{gal}}^2}{v}, \quad (5)$$

where $\ln \Lambda$ is the logarithm of the ratio of maximum and minimum impact parameters and M_{gal} is the mass of the galaxy. Using the same values as above, we obtain an energy loss of $\sim 6 \times 10^{42} \text{ erg s}^{-1}$, which is somewhat above the values derived for ram pressure heating. However, it is not clear how efficiently the energy is converted into heat. The accelerated gas may lead to propagating waves in the ICM that still need to be dissipated. In contrast, in the wake behind the galaxy, the ICM develops small-scale turbulence, which will dissipate locally.

Moreover, ram pressure heating scales with A_{proj} , whereas dynamical friction heating scales with M_{gal}^2 . Hence, for the large number of small galaxies ram pressure heating may prevail.

Our simulations indicate that a supersonic galaxy stirs the ICM much more than a subsonically moving galaxy. Hence, gas that cools significantly below the local galaxy velocity dispersion will be heated more efficiently.

Compared to ICM temperatures, the ISM lost from galaxies by ram pressure stripping is cold ($\sim 10^4 \text{ K}$) and thus might be considered an energy sink for the ICM. However, the energy that becomes available by decelerating this stripped gas can be used for its heating. Given that cluster galaxies move with typical velocities comparable to the ICM

sound speed, this energy approximately balances the energy needed to heat the stripped ISM to ICM temperatures.

5 SUMMARY

We ran high-resolution 3D hydrodynamical simulations of ram pressure stripping of a massive disc galaxy focussing on the evolution of the galaxy's wake. We combined the following parameters: a medium and a high ram pressure, one subsonic and one supersonic ICM velocity, inclinations of 30° and 75° . We traced the tail to a distance of 260 kpc behind the galaxy.

In our simulations, the wakes reached typical widths of ~ 60 to 100 kpc at distances of 100 kpc behind the galaxy. The widening proceeds systematically with opening angles $\lesssim 23^\circ$ in subsonic runs. Depending on the projection angle, subsonic wakes can show oscillations similar to von Karman vortex streets. The wakes in the supersonic cases also show widening, but in an irregular fashion.

We compared our simulations with the observed tail of NGC 4388. We could explain some features, but our simulated tails are wider than this observed one. We discussed possible reasons for this difference.

Finally, we provided suggestions how our simulation results could be used in cluster simulations that aim at predicting the evolution of the metal distribution in the ICM due to ram pressure stripping.

ACKNOWLEDGEMENTS

We acknowledge the support by the DFG grant BR 2026/3 within the Priority Programme "Witnesses of Cosmic History" and the supercomputing grants NIC 1927 and 1658 at the John-Neumann Institut at the Forschungszentrum Jülich. The simulations were produced with STELLA, the LOFAR BlueGene/L System. Special thanks for support go to H. Falcke.

The results presented were produced using the FLASH code, a product of the DOE ASC/Alliances-funded Center for Astrophysical Thermonuclear Flashes at the University of Chicago.

REFERENCES

- Abadi M. G., Moore B., Bower R. G., 1999, MNRAS, 308, 947
- Acreman D. M., Stevens I. R., Ponman T. J., Sakelliou I., 2003, MNRAS, 341, 1333
- Batchelor G. K., 2000, An introduction to fluid dynamics. Cambridge University Press
- Binney J., Tremaine S., 1987, Galactic Dynamics. Princeton University Press, Princeton, New Jersey
- Burkert A., 1995, ApJ, 447, 25
- Cayatte V., Kontanyi C., Balkowski C., van Gorkom J. H., 1994, AJ, 107, 1003
- Cayatte V., van Gorkom J. H., Kotanyi C., 1990, AJ, 100, 604
- Davies J., Minchin R., Sabatini S., van Driel W., Baes M., Boyce P., de Blok W. J. G., Disney M., Evans R., Kilborn V., Lang R., Linder S., Roberts S., Smith R., 2004, MNRAS, 349, 922
- Domainko W., Mair M., Kapferer W., van Kampen E., Kronberger T., Schindler S., Kimeswenger S., Ruffert M., Mangete O., 2005, A&A, ??, ??
- Faltenbacher A., Kravtsov A. V., Nagai D., Gottlöber S., 2005, MNRAS, 358, 139
- Fryxell B., Olson K., Ricker R., Timmes F. X., Zingale M., Lamb D. Q., MacNeice P., Rosner R., Truran J. W., Tufo H., 2000, ApJS, 131, 273
- Gavazzi G., Boselli A., Mayer L., Iglesias-Paramo J., Vilchez J. M., Carrasco L., 2001, ApJ, 563, 23L
- Gavazzi G., Contursi A., Carrasco L., Boselli A., Kennicutt R., Scodreggio M., Jaffe W., 1995, A&A, 304, 325
- Hernquist L., 1993, ApJS, 86, 389
- Kenney J. D. P., Koopmann R. A., 1999, AJ, 117, 181
- Kenney J. D. P., Koopmann R. A., 2001, in Hibbard J. E., Rupen M. P., van Gorkom J. J., eds, Gas and Galaxy Evolution Vol. 240 of ASP Conf. Ser., Environmental effects on gas and star formation in virgo cluster spiral and peculiar galaxies. ASP, San Francisco, p. 577
- Kenney J. D. P., van Gorkom J. H., Vollmer B., 2004, AJ, 127, 3361
- Kim W., El-Zant A. A., Kamionkowski M., 2005, ApJ, 632, 157
- Koopmann R. A., Haynes M. P., Catinella B., 2005, AJ, in press, astro-ph/0510374
- Koopmann R. A., Kenney J. D. P., 1998, ApJ, 497, 75L
- Koopmann R. A., Kenney J. D. P., 2004a, ApJ, 613, 866
- Koopmann R. A., Kenney J. D. P., 2004b, ApJ, 613, 851
- Marcolini A., Brighenti F., A.D'Ercole 2003, MNRAS, 345, 1329
- Miyamoto M., Nagai R., 1975, PASJ, 27, 533
- Mori M., Burkert A., 2000, ApJ, 538, 559
- Oosterloo T., van Gorkom J., 2005, A&A, 437, L19
- Ostriker E. C., 199, ApJ, 513, 252
- Quilis V., Moore B., Bower R., 2000, Science, 288, 1617
- Reynolds C. S., McKernan B., Fabian A. C., Stone J. M., Vernaleo J. C., 2005, MNRAS, 357, 242
- Roediger E., Brüggen M., 2006, MNRAS, submitted, astro-ph/0512365
- Roediger E., Hensler G., 2005, A&A, 433, 875
- Schindler S., Kapferer W., Domainko W., Mair M., van Kampen E., Kronberger T., Kimeswenger S., Ruffert M., Mangete O., Breitschwerdt D., 2005, A&A, 435, L25
- Schulz S., Struck C., 2001, MNRAS, 328, 185
- Solanes J. M., Manrique A., García-Gómez C., González-Casando G., Giovanelli R., Haynes M. P., 2001, ApJ, 548, 97
- Stevens I. R., Acreman D. M., Ponman T. J., 1999, MNRAS, 310, 663
- Takizawa M., 2005, ApJ, 629, 791
- Vollmer B., Beck R., Kenney J. D. P., van Gorkom J. H., 2004, AJ, 127, 3375
- Vollmer B., Braine J., Balkowski C., Cayatte V., Duschl W. J., 2001, A&A, 374, 824
- Vollmer B., Cayatte V., Balkowski C., Duschl W. J., 2001, ApJ, 561, 708
- Vollmer B., Cayatte V., Boselli A., Balkowski C., Duschl W. J., 1999, A&A, 349, 411

Vollmer B., Huchtmeier W., 2003, *A&A*, 406, 427

This paper has been typeset from a \TeX / \LaTeX file prepared by the author.